Soft Matter

PAPER

View Article Online
View Journal | View Issue

Cite this: *Soft Matter*, 2015, 11, 6872

Glancing angle metal evaporation synthesis of catalytic swimming Janus colloids with well defined angular velocity†

R. J. Archer, A. I. Campbell and S. J. Ebbens*

Received 29th May 2015,
Accepted 27th July 2015

DOI: 10.1039/c5sm01323b

www.rsc.org/softmatter

The ability to control the degree of spin, or rotational velocity, for catalytic swimming devices opens up the potential to access well defined spiralling trajectories, enhance cargo binding rate, and realise theoretically proposed behaviour such as chiral diffusion. Here we assess the potential to impart a well-defined spin to individual catalytic Janus swimmers by using glancing angle metal evaporation onto a colloidal crystal to break the symmetry of the catalytic patch due to shadowing by neighbouring colloids. Using this approach we demonstrate a well-defined relationship between the glancing angle and the ratio of rotational to translational velocity. This allows batches of colloids with well-defined spin rates in the range 0.25 to 2.5 Hz to be produced. With reference to the shape and thickness variations across the catalytically active shapes, and their propulsion mechanism we discuss the factors that can lead to the observed variations in rotational propulsion.

Introduction

Micron scale swimming devices (microswimmers) can generate translational displacements in excess of those produced by passive Brownian diffusion. Using catalysis rather than deformations to propel such devices has to date been the only approach that has resulted in autonomous motion without external actuation. This is due to the requirement for non-reciprocal motion imposed by low Reynolds number fluids[1] which has so far proven too difficult to autonomously produce. Catalytic devices are often driven by surface decomposition of dissolved fuel by a spatially defined asymmetrical distribution of catalyst. Many variants of micron scale swimming devices exist,[2] prominent examples include bi-metallic nanorods[3] and Janus colloids, Fig. 1.[4] Potential applications for autonomous micro scale swimming devices include microfluidic transport;[5,6] where the ability to selectively bind and transport cancer cells has been demonstrated,[7] and drug delivery, where enhanced transport combined with smart release behaviours could improve active ingredient potency and selectivity.[8] Motivated by these goals, most current autonomous swimming devices have been designed to produce intrinsically linear propulsion trajectories within the constraints of unavoidable Brownian rotational diffusion which causes randomisation of their orientation with time.

For example, in the case of a Janus colloid, catalytic decomposition carried out by a rotationally symmetrical catalytic hemisphere, such as that shown in Fig. 1, results in purely translational thrust propulsion orientated away from the active coated hemisphere.[9] This leads to trajectories exhibiting linear propulsion until Brownian rotational diffusion randomises orientation.[4] Likewise, bimetallic nanorods intrinsically produce translational rather than rotational propulsion.

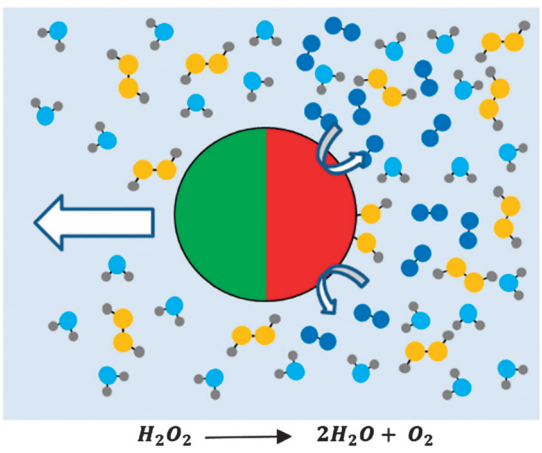

Fig. 1 Catalytic Janus swimmer schematic, the catalytically active hemisphere (red) generates thrust when in solution of dissolved hydrogen peroxide fuel (orange), producing water (light blue) and oxygen (dark blue), resulting in motion away from the cap.

Department of Chemical and Biological Engineering, The University of Sheffield, Mappin Street, Sheffield S1 3JD, UK. E-mail: s.ebbens@sheffield.ac.uk

† Electronic supplementary information (ESI) available. See DOI: 10.1039/c5sm01323b

However, it has become clear that there are additional application areas and fundamental investigations that could be enabled by the ability to produce swimming devices with well-defined spiralling and spinning trajectories, necessitating the development of methods to produce rotational propulsion. As an example of the potential for rotating devices, micron sized spinning colloids have been shown to influence the directional growth of neurons *in vitro*,[10] induce cell death by bursting lysosomes through the generation of shear forces,[11] and enhance surface protein binding rates.[12] However, these demonstrations required external actuation of the rotational behaviour, achieved *via* applying circularly polarized light with angular momentum to an optically trapped bead, using dynamic magnetic fields to rotate superparamagnetic iron oxide nanoparticles, and the rotation of magnetic colloids using a quadrupole magnet respectively. Another tested scheme for inducing rapid rotation assembled arrays of nanowire rotors onto patterned nanomagnetic bearings, actuated by quadrupole microelectrodes, which resulted in controlled rotation over 18 000 rpm.[13] In addition, ultrasonically actuated gold nanorods have been shown to rotate at kilohertz speeds around their long axis, generating localised microvortical flows in tracer particles.[14] However, in each case, relying on external actuation to induce colloidal rotation imposes potential limitations on associated applications, due to the complexity of the field generating apparatus. This motivates the quest to produce autonomous rotations based on catalytic fuel decomposition and remove the requirement for external actuation: the focus of this study. Realising such rotating devices would also allow interesting phenomena proposed for self-motile rotor/translators to be experimentally accessed. These include chiral diffusion effects,[15] predication for reversal of rotation direction in confined geometry,[16] and proposals for novel sorting methods.[17] An extra motivation for investigating autonomous rotation is provided by the potential for devices that can transition from linear running to rapid rotation to emulate the chemotaxis behaviour displayed by bacteria in order to respond to local stimuli gradients.[18]

Despite these potential benefits, modifying autonomous microswimmers to impart controlled rotational behaviour has received relatively little attention. One approach is to utilise shape asymmetry, for example it has been shown that L-shaped swimming devices can generate an asymmetric velocity dependant torque, resulting in circular trajectories.[19] This study required light actuation to induce device motion *via* localised heating at a metallic strip coated on the polymeric device body, but the principle could also be applied to autonomous devices. However, there are some drawbacks for this method, including the difficulty in mass-producing appropriately shaped devices. In some early reports, self-propulsive nanorods were observed to undergo tight rotations, however this was ultimately found to be due to them becoming randomly stuck to substrate defects, and was not well controlled.[20] However, nanorods exhibiting fast autonomous rotation were subsequently manufactured using a complex tri-metal arrangement that allowed hydrodynamic interactions between pairs of rotors to be observed.[21] Again, these devices are relatively difficult to manufacture, and due to their metallic structure rapidly sediment preventing them exhibiting motion throughout bulk solutions. Considering Janus catalytic devices, research has previously shown that agglomerated dimers rotate with a frequency dependant on the relative cap orientation between Janus colloids.[18] However, the dimer orientations were not controllable during the agglomeration process leading to a wide distribution in rotational frequencies.[4] A small degree of additional propulsive spin, was also noted in the original report for hemispherical platinum coated Janus swimmers, where calculated rotational diffusion times were found to be faster than expected for purely translational velocity. This was suggested to be due to physical imperfections in the active cap. One potential additional advantage for further investigating rotational phenomena for this Janus colloid system is the recently reported gravitaxis effects, which can impart a directional bias to otherwise isotropic trajectories, and so if combined with spin could allow access to a range of 3D orientated helical behaviours.[22]

In this context, here we propose to investigate the effect of systematically breaking the symmetry for the hemispherical active layer in Janus catalytic spheres as a potential route to impart well defined spin, or rotational velocity. While the effect of breaking the rotational symmetry for such devices has not been the subject of any specific theoretical treatment, the recent proposal that an electrokinetic mechanism dominates in Janus swimmers, suggested that catalyst thickness variations from the hemispheres' pole to the equator of the deposited layer cause reactivity variations which drive fluid pumping around the swimmer body.[23] Consequently, modifying this flow by removing sections of the reactive cap may provide a route to induce driven rotations. To break the cap symmetry in this way we employ a glancing angle metal evaporation technique developed by Pawar and Kretzschmar to deposit the active platinum catalyst.[24] In this scheme, colloids were assembled into close packed colloidal crystals and exposed to a directional metal vapour from a well-defined glancing angle. The oblique deposition angle allows colloids to exert shadowing effects on each other, breaking the symmetry through the deposited hemisphere to a variable extent controlled by the glancing angle, and thereby allowing a high level of control over cap shape and coverage. Using this approach we systematically vary the glancing angle, characterise the active cap shapes, and track the resulting propulsive trajectories. Established mean-square displacement analysis[25] is then applied to these trajectories to quantify both translational and rotational velocity components. This allows a correlation between cap structure and propulsion character to be made. Finally a discussion of the origin of the observed behaviour based on proposed propulsion mechanisms and the calculated catalyst thickness distributions is made.

Experimental details

Materials

Platinum wire of 0.25 mm (99.99%), ethanol (99.98%) and H_2O_2 (puriss grade, 30% w/w) were purchased from Sigma Aldrich.

Carboxyl terminated polystyrene microspheres (1.9 μm, 4% w/w in water) were bought from Invitrogen. All materials were used as received. Deionised (DI) water was obtained from an Elga Purelab Option filtration system (15 MΩ cm).

High density colloidal crystals

Monolayers of hexagonally close packed carboxyl terminated polystyrene microspheres were prepared by self-assembly at an air/water interface as described by Weekes *et al.*[26] Briefly, the stock solution of carboxyl terminated polystyrene microspheres was diluted with ethanol (1 : 1). The diluted solution was spread slowly across a glass slide partially submerged in DI water and angled at approximately 45° relative to the water surface. The diluted solution of carboxyl terminated polystyrene microspheres spreads down the slide to the meniscus of the DI water where upon they spread across the surface as a monolayer and assemble into the colloidal crystal hexagonal close pack array. These floating crystals are scooped up on to glass slides and left to dry under ambient conditions.

Low density colloid dispersion

Low density, well separated arrangements of carboxyl terminated polystyrene microspheres were prepared by spin coating (2000 RPM) low concentration solutions of the stock bead solution, diluted with ethanol (1 : 4000), onto cleaned glass microscope slides.

Metal deposition

Platinum metal was coated onto the prepared slides containing either high density colloidal crystals or low density spun coat microspheres by e-beam evaporation of the source platinum metal using a Moorfield Minilab 80 e-beam evaporator under high vacuum, (1×10^{-9} bar). Platinum films were deposited to an approximate thickness of 10 nm, measured using a quartz crystal monitor. E-beam evaporation under these conditions is highly directional and coats only by line of sight, therefore (for unshadowed colloidal particles) coats only the exposed hemisphere giving the desired Janus particles with catalytic activity.

Angle control

Angles reported here are relative to the source metal with 90° being perpendicular and 0° being parallel to the path of the ejected metal vapour during e-beam evaporation. During e-beam evaporation the prepared samples of carboxyl terminated polystyrene microspheres on glass microscope slides are held at angles from 90° to 10°. This is achieved through use of a purpose built microscope slide holder on a rotatable axis, held within a metal frame. The angle is set manually before loading into the vacuum chamber of the e-beam evaporator.

2D Tracking

Platinum coated colloids were transferred to solution using damp lens tissue to physically rub the microscope slides, displacing the particles from the surface and into the tissue. The tissue is transferred into a small (ml) volume of DI water and shaken to release the Janus particles into solution. The solution is transferred to a clean vial without the tissue. An initial cleaning step is employed to remove contaminants from the platinum cap surface by the addition of hydrogen peroxide (1 : 1) to make a 15% w/w H_2O_2 solution, this solution is sonicated in a sonic bath for 5 minutes and left to stand for a further 25 minutes after which the solution is diluted with additional DI water (2 : 1) to 10% w/w H_2O_2 in which the measurements will take place.

Tracking of the synthesised self-motile particle was performed using a Nikon eclipse inverted microscope fitted with a Pixelink PL-B742F camera. Videos of 1000 frames recorded at 33 fps at a resolution of 640 × 480 were taken of the swimming device in 10% H_2O_2 and the videos were analysed using custom built software based on LabVIEW vision assistant which gives frame by frame x, y coordinates of the swimming devices and their mean square displacements by time.

Results

Firstly we concentrate on the structure of the catalytic caps deposited by glancing angle deposition. Fig. 2 shows schematically the possible shadowing effects and important parameters for glancing angle metal evaporation. Fig. 2a and b make it apparent that for any shadowing to occur, colloids must be in close proximity. For this reason we performed catalyst evaporation for variable glancing angles, θ, on a hexagonal close packed colloidal monolayer, which provides a regular well defined colloidal

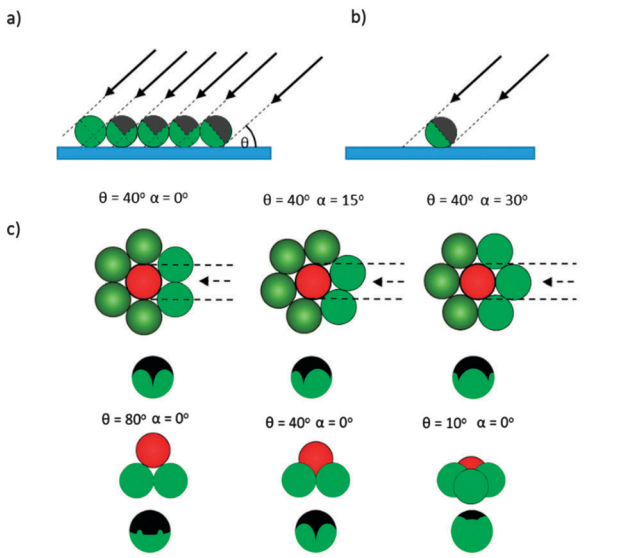

Fig. 2 (a) Glancing angle evaporation onto a colloidal crystal modifies the cap shape as the glancing angle (θ) is varied due to the potential for neighbouring colloids to shadow the line of sight path of the metal (black shading, arrows indicate direction of metal source). (b) If colloidal coverage is sufficiently sparse, changing the glancing angle, θ, will not affect the deposited cap shape which will remain hemispherical. (c) Top section: at a fixed glancing angle, the orientation of the colloidal crystal (α) relative to the metal source will produce variations in the deposited cap shape. The resulting deposited metal pattern on the red-sphere is shown below, light green spheres are responsible for the shadowing effects. Bottom section: the effect of varying glancing angle for a fixed crystal orientation is depicted. As the glancing angle is reduced, the patch coverage is reduced, and the perimeter shape is also altered.

arrangement with predictable shadowing features. In addition, we also prepared samples at sparse coverage, to provide a control sample, where no cap shape alteration was expected, Fig. 2b. Fig. 2c shows how when depositing metal from a glancing angle onto a colloidal crystal, both the glancing angle θ and the crystal orientation α will affect the perimeter shape of the deposited cap. While reducing θ is expected to considerably reduce the coverage of the deposited metal due to increased shadowing, variations in α at a given θ value have a more subtle effect, changing the symmetry and position of the cusp like features that define the cap perimeter (Note: all these features are also fully explained, modelled and experimentally verified in the Pawar and Kretzschmar study). Fig. 3a shows an optical microscopy image of a colloidal crystal section generated by the method described above by Weeks *et al.* This image shows that the apparently continuous colloidal crystal generated is in fact polycrystalline consisting of multiple hexagonally close packed domains of around 20–30 μm^2 regions. The boundaries between the crystallite regions are densely packed but do not have a well defined or predictable arrangement of colloids, however, these regions represent a small fraction of the overall colloidal crystal so the majority of colloids are expected to be regularly shadowed as outlined above. With the geometric model from Fig. 2 for the expected cap shapes, we can consider Fig. 3b–f which depicts back scattered Scanning Electron Microscope (SEM) images for small regions of colloidal crystal after metal deposition at a series of decreasing glancing angles. In these back scattered images, regions covered by platinum metal appear brighter than the uncoated colloids. Fig. 3b–f shows the effect of glancing angle viewed from the top down SEM images for colloidal crystals. As glancing angle decreases, the bright contrast indicating the distribution of platinum metal across each colloid becomes visibly asymmetric, indicating shadowing has occurred. This asymmetry is aligned across the entire colloidal crystal (and does not rotate with the scan direction, ruling out charging artefacts), and is orientated with respect to the direction of the metal source relative to the colloidal crystal orientation (marked by red arrows). At lower glancing angles, the asymmetry is increasingly pronounced as more of the directional metal vapour is shadowed by a given colloids' neighbours. While Fig. 3b–f depict single crystal regions of colloidal crystal, suggesting that α is well defined, the colloidal crystal regions generated by the float method used to prepare the substrate are in fact polycrystalline over larger regions, Fig. 3a. Consequently, when particles are re-suspended from the substrate into solution, either for further SEM observation or to allow observations of catalytic propulsion, this will result in many different crystalline domains being sampled, leading to the crystal orientation angle α being uncontrolled and randomised in this current experiment.

To further verify the perimeter shape of the cap, the contents of each colloidal crystal were dispersed into water, then, re-deposited and re-examined by SEM, to randomise the viewing angle. Fig. 3g shows randomly orientated colloids from the ($\theta = 90^\circ$) crystal, and for the colloids lying "sideways" on a smooth unbroken equatorial cap boundary is observed, this is consistent with the expectation that normal evaporation will not produce any shadowing effects. Fig. 3h–k show the perimeter of the cap for

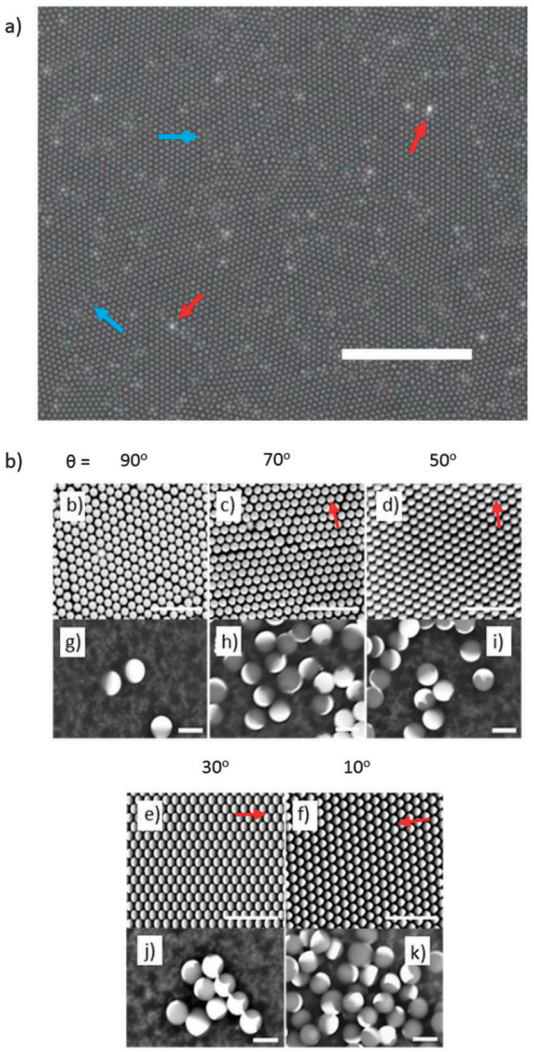

Fig. 3 (a) Optical microscopy image of Pt coated colloidal crystal, red arrows indicate defect sites in the crystal, blue arrows mark examples of crystalline grain boundaries. Scale bar represents 40 μm. (b–k) Back-scattered SEM images following glancing angle platinum deposition onto a colloidal crystal of 1.9 μm diameter carboxylated polystyrene particles. Pt coated colloidal crystals after evaporation at angles of 90°, 70°, 50°, 30° and 10°, (b–f) respectively where the scale bar represents 10 μm. Red arrows are used to mark the direction of the incoming platinum vapour where it was apparent. (g–k) Colloids prepared at glancing angles 90°, 70°, 50°, 30° and 10° after dispersal and re-deposition of the colloidal crystals shown in (c–g), the scale bars represent 2 μm.

samples prepared at decreasing glancing angles, where shadowing is predicted. At a glancing angle of 70°, small deviations in the equatorial cap perimeter line are seen for some particles, where near neighbours have shadowed the metal deposition, Fig. 3h. Other particles lying at different randomised orientations display smooth equatorial perimeters. This is as expected, because, each individual Janus particle will have one side facing towards the metal source which is shadowed by neighbouring colloids, whereas the other side of the caps' shape is masked by the particle itself, Fig. 2c. As the glancing angle is decreased, the deviations in perimeter on the side facing the evaporation source become more pronounced, however again some of the smoother, trailing edge

perimeter can be seen at other orientations. These perimeter features show good agreement with the expected variations shown in Fig. 2c. Finally, SEM examination of the sparse coverage colloids (not shown) confirmed that complete hemispherical caps were deposited at all glancing angles.

Consistent with previous reports, when the catalytically active Janus colloids prepared using this method were re-suspended into 10 wt/v% hydrogen peroxide solutions and examined under a microscope, enhanced motion due to the asymmetrical decomposition of fuel molecules was apparent (Fig. 1). Initial qualitative comparisons of the different batches of Janus catalytic swimmers showed a striking difference in motion character, with batches prepared at lower glancing angles visibly exhibiting increasingly tight circling trajectories. Videos included in the ESI† (S1) illustrate these differences. Frame by frame tracking of the position of the colloids in these videos enabled the construction of *xy* trajectory plots, Fig. 4a. For normal (θ = 90°) deposition, the trajectories resemble those reported previously for similar sized Janus swimmer colloids, exhibiting enhanced motion significantly exceeding the displacements observed for unfuelled colloids in water. The trajectories show linear runs, followed by direction changes which have been previously explained by the finding that translational propulsive thrust direction is correlated to swimmer orientation, which is subject to Brownian rotational diffusion. However, as the glancing angle decreases, a dramatic change in trajectory character is observed: increasingly tight spiralling is induced. This suggests that the asymmetry introduced by shadowing effects is resulting in the introduction of increasing amounts of angular propulsive velocity while still maintaining a translational propulsive thrust too. In contrast, the sparsely coated spin coated colloids do not show significant variation in trajectory as a function of glancing angle (ESI,† S2).

To quantify this effect, it has been previously shown that for the case of a freely diffusing colloid producing both angular and rotational velocity, the temporal evolution of Mean Squared Displacements (MSD) are given by eqn (1).

$$\Delta L^2(t) = 4Dt + \frac{2v^2 D_r t}{D_r^2 + \omega^2} + \frac{2v^2(\omega^2 - D_r^2)}{(D_r^2 + \omega^2)^2} + \frac{2v^2 e^{-D_r t}}{(D_r^2 + \omega^2)^2}\left[(D_r^2 - \omega^2)\cos\omega t - 2\omega D_r \sin\omega t\right] \quad (1)$$

This expression contains the Brownian translational diffusion coefficient (D), and rotational diffusion constant (D_r) in addition to the translational (v) and the angular velocity (ω) which can consequently be extracted by fitting to the experimental data.[25] Therefore, to quantify both the angular velocity and the translational velocity, mean squared displacement (MSD) plots for each recorded trajectory were generated, with typical fitted examples displayed in Fig. 4. For samples prepared by normal evaporation, MSD plots consistently fit to eqn (1) with ω at or close to zero, reflecting that MSD evolution is determined by the Brownian diffusion properties and that the translational velocity direction is solely being rotated by stochastic effects, with no driven propulsive rotation. However, as glancing angle decreases, oscillations in the MSD are seen which increase in frequency, and are well fitted with increasing values of ω, reflecting the ability of glancing angle evaporation to induce driven rotations of the propulsive trajectory, presumably through rotating the Janus colloids' orientation.

Translational and angular velocities were determined in this way for many trajectories from each batch of prepared colloids, Fig. 5a and b (3 separately prepared samples at each glancing angle were analysed and >20 trajectories from each of these were analysed). The average translational velocity for Janus particles suspended from a colloidal crystal is 16.48 (±4.40) μm s^{-1}, while sparse coverage spin coated prepared samples give a mean value of 12.28 (±0.69) μm s^{-1}. For the spun coat samples velocity appears to be unaffected by the glancing angle, as expected due to their symmetrical hemispherical cap. However, significantly higher translational velocities are observed for some of the colloidal crystal samples, particularly for glancing angles in the range 20°–40°. Considering average rotational velocity, Fig. 5b, an increase in ω with decreasing glancing angle from 1.16 to 16.46 rad s^{-1} (corresponding to 0.25 to 2.62 Hz rotational frequency) peaking at θ = 20°

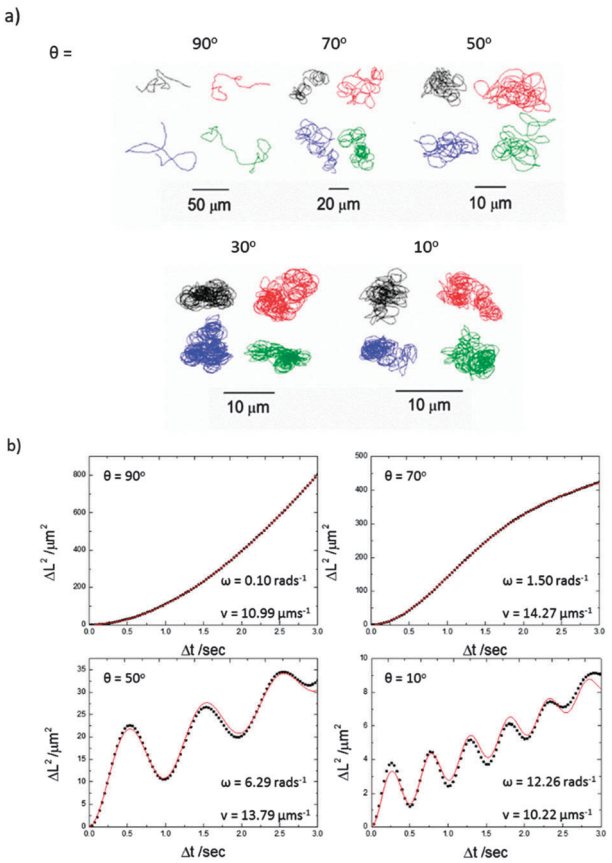

Fig. 4 (a) Representative *xy* plot trajectories (30 seconds) for 1.9 μm diameter Janus colloids re-dispersed into 10% H_2O_2 solutions after platinum evaporation onto a colloidal crystal at a range of glancing angles. (b) Representative MSD plots from Δt 0.0 to 3.0 seconds for microswimmers prepared from colloidal crystals at 90°, 70°, 50° and 10° θ, (a–d) respectively. Black points represent experimental data and the red line is generated from eqn (1) to find ω and v.

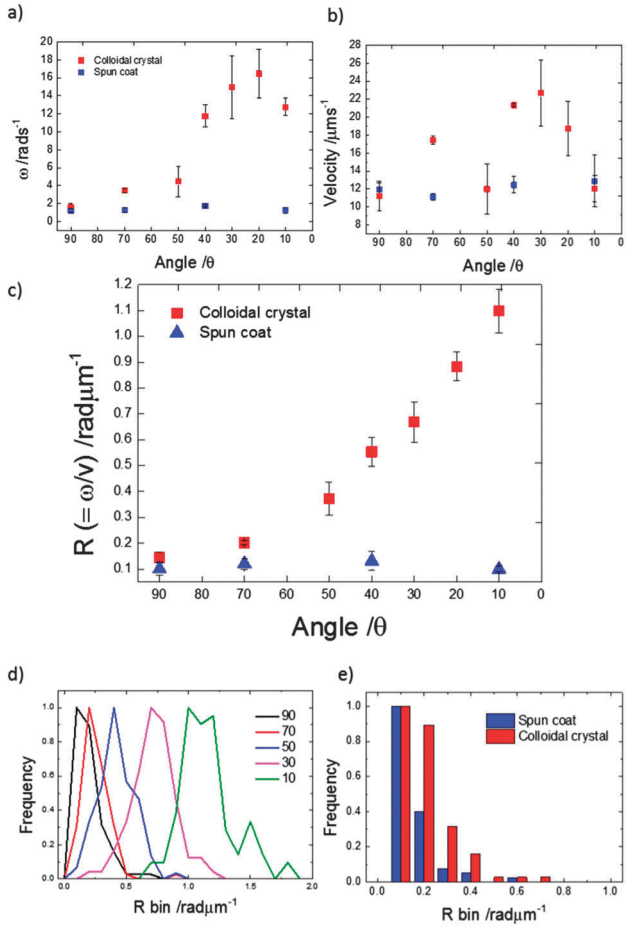

Fig. 5 (a). Angular velocity (ω) profile of microswimmers prepared from colloidal crystals (red) and sparsely spun coat colloids (blue) for a range of angles from 0° to 80° θ. (b) Velocity (v) profile of microswimmers prepared from colloidal crystals (red) and sparsely spun coat colloids (blue) for a range of angles from 90° to 10° θ (c) Ratio (R) between ω and v for microswimmers prepared from colloidal crystals (red) and sparsely spun coat colloids (blue) for a range of angles from 90° to 10° θ. (d) R value distribution of microswimmers prepared from colloidal crystals for angles of 90° (black), 70° (red), 50° (blue), 30° (pink) and 10° (green) θ. (e) R value distribution for microswimmers prepared from spin coating (blue) and colloidal crystals (red) at 90° θ.

is observed. In comparison, spun coat prepared samples with a sparse colloidal distribution where no shadowing is expected, give a mean ω of 1.32 ($\pm$0.28) rad s^{-1} (0.21 Hz) and the glancing angle makes no significant change to ω. Due to the variations in translational velocity as a function of glancing angle for colloidal crystal samples, it is instructive to also consider the derived parameter, $R = \frac{\omega}{v}$. R represents the number of radians turned by a given Janus colloid per unit translational distance travelled, and so gives a measure of how tightly spinning the trajectory of an average colloid prepared under a given condition is, irrespective of the absolute magnitudes of ω and v. This is useful to ascertain the relative production of translational and rotational velocity for a given batch of colloids. Fig. 5c, shows that R increases monotonically with a reduction in the glancing angle θ, whereas for spun coat samples there is no link between R and θ. This demonstrates the potential to use the glancing angle deposition method to reproducibly prepare batches of Janus colloids with a well-defined trajectory character. Fig. 5d shows the frequency distributions for the R values as a function of glancing angle to illustrate the degree of control achieved.

Fig. 5e presents a tightly binned R value frequency distribution comparison for Janus colloids prepared from spin coating and colloidal crystals both at 90° glancing angle (*i.e.* normal evaporation). This data reveals that swimmers prepared by sparse coverage spin coating have slightly lower R values, indicating more persistent trajectories, compared to those prepared from a colloidal crystal, despite the equivalence in coating direction. In any case, both samples still show a small driven rotation (R = 0.10 ($\pm$0.09) and 0.14 ($\pm$0.11)) component, which presumably reflects the experimental limit for attempts to manufacture a perfectly symmetrical platinum cap using metal evaporation, as discussed below.

Discussion

To understand the origin of the variable amount of driven rotation introduced by depositing the platinum cap at glancing angles, it is first instructive to summarise two proposed motion producing mechanisms for catalytic Janus spheres. Note that we exclude considering bubble propulsion[29] from this discussion based on the absence of experimental evidence for any bubble nucleation at the catalytic surface coating, which would also be energetically unfavourable due to the high surface curvature.[30] The originally proposed diffusiophoretic model states that in a standard case of a full hemispherical active cap, motion is generated due to a self-generated concentration gradient in the interfacial region of the colloid, with the resulting force being proportional to the concentration of a generated product at the surface of the catalyst; in comparison to the concentration of the product in the bulk solution.[27,28] This theory was developed under the expectation that the catalytic activity across the active hemisphere is uniform. However, recent measurements for the dependency of propulsion velocity on dissolved salt concentration indicated that pure diffusiophoresis is actually a minor contribution to propulsion for evaporatively produced Janus colloids, and instead suggests an electro kinetic mechanism is dominant.[23] Rather than considering the Janus catalytic hemisphere as having uniform activity, a driving force for electrokinetic propulsion is the existence of a catalytic reactivity gradient across the active coating. The potential for such a gradient to exist was suggested by experiments which show the thickness of an evaporated platinum coating has a significant effect on the rate of decomposition, particularly in the region 0–10 nm.[23] Fig. 6a shows a 3D schematic of the thickness variations predicted for a Janus colloid subject to 10 nm normal metal evaporation (θ = 90° – See ESI† S3, for details about how these thickness variation plots were obtained). It is apparent that while the pole of the coated hemisphere receives the full 10 nm thickness coating, there is a thickness gradient towards the equatorial region which receives only a vanishingly thin

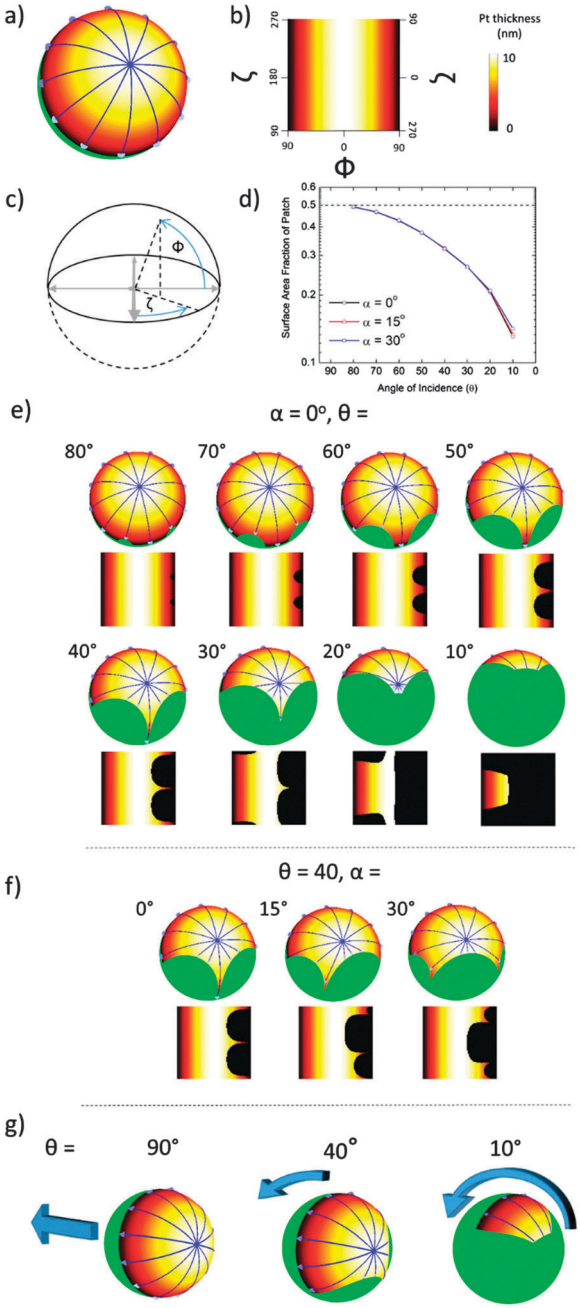

Fig. 6 (a) 3D model of a Janus swimmer without shadowing. (b) Cap shape and thickness diagram represented in unwrapped 2D format using altitude and azimuthal coordinates and colour representation plot of platinum cap thickness from 0 to 10 nm. (c) Schematic representation of the altitude Φ and azimuthal ζ angles. (d) Graphical representation of overall patch area coverage with θ for alpha (0°, 15° and 30°). (e) 3d and 2d representation of the cap (same format as a and b) for θ = 80° to 10° at α = 0. (f). 3d and 2d representation of the cap (same format as a and b) for α = 0°, 15° and 30° at θ = 40°. (g) Schematic representation of changing cap shape.

metal coating at the cap perimeter. A 2D ''unwrapped'' representation for these thickness variations, described using polar coordinates (Fig. 6c) is shown in Fig. 6b, where the pole lies along the Φ = 0° line, and the equatorial perimeter along the Φ = 90° line, in addition a colour gradient chart relating to cap thickness is given. Using the analysis proposed for an electrokinetic mechanism, these variations will lead to pole-equator reaction rate gradients generating electrophoretic motion. Fig. 6a shows motion lines from high (polar-blue circle) to low (equatorial) reactivity/thickness: which reflect the expected direction of motion for the colloid. These lines, and the corresponding thickness variations' symmetry about Φ = 0° in the 2D plots, suggests that for a complete hemisphere the colloids propulsion will be rotationally symmetrical, leading to the expectation of no rotational velocity, and pure translation. This is confirmed by our experiments within the limits that we can produce a perfectly symmetrical metal hemisphere. We now consider the effect of reducing the glancing angle on the cap shape and activity distribution, and implications for electrophoretic motion. Fig. 6e shows the effect of reducing glancing angle on 3D and 2D visualisations of the catalytic cap. This series is shown for a fixed colloidal crystal orientation (α = 0°). It is apparent that shadowing increasingly breaks the symmetry of the deposited cap. Based on the argument above, the predicted electrophoretic propulsion force, indicated by the blue arrows, is progressively unbalanced across the cap, as the symmetry of the thickness gradient around Φ = 0° is broken. This provides a clear indication of how reducing glancing angle colloidal crystal batches can produce increasing amounts of angular velocity in the range θ = 90° to 20°, Fig. 5a. Of further note is that at the lowest glancing angle, θ = 10°, although the predicted motion lines are now entirely unbalanced, the maximum metal thickness is now also reduced below 10 nm, due to the pole of the deposited catalyst being shadowed. It is possible that this reduction in magnitude for the maximal thickness/activity explains the observed reduction in angular velocity for this batch. While the possible effect of these variations on translational velocity is complex, it is instructive to consider the extent to which the glancing angle also reduces the total coverage of active material, below 0.5 (50%), Fig. 6d, which could be expected to be a relevant parameter. Experimental data only shows an appreciable reduction in translational velocity when θ < 30°, *i.e.* when coverage reduces from around 0.28 to 0.14. There is a relative insensitivity of translational velocity to catalyst coverage in the region 0.5–0.28 coverage, and even some indication of lower coverage increasing translational velocity.

The remaining parameter to consider is the colloidal orientation, α. Fig. 6f, shows the effect of performing glancing angle deposition at a fixed value of θ, but at different values of α. It can be see that for example when α = 15°, the symmetry of the cap thickness variations around a second rotational axis (*i.e.* about ζ = 0°) is also removed. The corresponding 3D schematics show how this is likely to lead to a change in the rotational axis, compared to the case for angles of α where symmetry about ζ is retained (see 0° and 30°). However, it is qualitatively suggested by this simple geometric analysis, that the overall variations in the degree of symmetry breaking about ζ = 0° for different values of α are small compared to the effect of symmetry about Φ = 0° on steps of 10° in glancing angle

(See ESI† S5–S7 for schematic depicting many more examples). In addition, α has very little effect on overall catalyst coverage, Fig. 6d. This is consistent with the experimental data, which we believe to have been averaged over many values of α, a parameter over which we had no control, and yet despite this results in well separated angular velocity values for each batch. However, we note that an interesting extension to this work in the future would be to attempt to control α, for example by employing electrostatic methods to produce large orientated colloidal crystals. Finally, while this analysis has been based on the recent electrokinetic mechanism for Janus colloid motion, it is likely that the general rotational symmetry breaking arguments discussed here would be equally relevant to diffusiophoretic systems, however at present there is no model that considers the effect of asymmetrical reactivity gradients for this case.

Conclusions

Here we demonstrate the ability to use glancing angle metal deposition to control the catalyst cap geometry and trajectory for Janus colloids capable of producing autonomous motion by decomposing surrounding hydrogen peroxide fuel molecules. We highlight, that for glancing angle deposition onto a colloidal crystal, controlling the glancing angle θ alone allows batches of self-motile colloids with well-defined ratios of angular to translational propulsion velocity; and that the rate of rotation per unit length of translational motion varies monotonically with glancing angle, a relationship which in itself is of interest and further study of which may reveal insight into the phoretic mechanism. This simple method allows access to a range of autonomous trajectories, with rotational frequencies up to 3 Hz. These maximal rotational values exceed those obtained previously by allowing individual Janus colloids to self-assemble,[25] as well as resulting in tight rotational frequency distributions which were previously unobtainable. Individual self-motile rotating colloids provide the potential to develop new applications including mixing, as well as having the potential to interact with biological systems, where rotating colloids can induce cell death and direct structural developments. In the shorter term, it is hoped that this method for active colloid production may assist the verification of theoretically proposed phenomena such as confinement and chiral diffusion. In addition we note that these colloids remain in suspension and move in three-dimensions and so can potentially allow the interaction between spin and effects such as gravitaxis to be determined.

We explain the observed phenomena based on the electrokinetic mechanism for Janus catalytic colloid propulsion, and simple analysis of the shape, thickness and coverage variations for the deposited cap shape. This analysis shows that while the colloidal crystal orientation, α, is not the main parameter in determining rotational behaviour, the ability to manufacture batches of colloids at a well-defined orientation in the future could lead to even more control over the trajectories, and provide a method to also modify the axis of rotation.

Acknowledgements

We give thanks and appreciation to Prof. Ramin Golestanian for the MSD model used for oscillating displacements, to Dr Jonathan Howse for the 2D tracking software, Steven Blackburn for constructing a slide holder with adjustable angle, David Gregory for useful discussions, and to the EPSRC for funding this work through Dr Stephen Ebbens (EP/J0024021/1).

References

1 E. M. Purcell, *Am. J. Phys.*, 1977, **45**, 3–11.
2 R. Kapral, *J. Chem. Phys.*, 2013, **138**, 020901.
3 W. F. Paxton, A. Sen and T. E. Mallouk, *J. Chem.*, 2005, **11**, 6462–6470.
4 J. Howse, R. Jones, A. Ryan, T. Gough, R. Vafabakhsh and R. Golestanian, *Phys. Rev. Lett.*, 2007, **99**, 048102.
5 J. Burdick, R. Laocharoensuk, P. M. Wheat, J. D. Posner and J. Wang, *J. Am. Chem. Soc.*, 2008, **130**, 8164–8165.
6 S. Sundararajan, P. E. Lammert, A. W. Zudans, V. H. Crespi and A. Sen, *Nano Lett.*, 2008, **8**, 1271–1276.
7 S. Balasubramanian, D. Kagan, C.-M. J. Hu, S. Campuzano, M. J. Lobo-Castañon, N. Lim, D. Y. Kang, M. Zimmerman, L. Zhang and J. Wang, *Angew. Chem., Int. Ed.*, 2011, **50**, 4161–4164.
8 D. Patra, S. Sengupta, W. Duan, H. Zhang, R. A. Pavlick and A. Sen, *Nanoscale*, 2013, **5**, 1273–1283.
9 S. J. Ebbens and J. R. Howse, *Langmuir*, 2011, **27**, 12293–12296.
10 T. Wu, T. A. Nieminen, S. Mohanty, J. Miotke, R. L. Meyer, H. Rubinsztein-Dunlop and M. W. Berns, *Nat. Photonics*, 2011, **6**, 62–67.
11 E. Zhang, M. F. Kircher, X. M. Koch, L. Eliasson, S. N. Goldberg and E. Renstrom, *ACS Nano*, 2014, **8**, 3192–3201.
12 A. van Reenen, A. M. de Jong and M. W. J. Prins, *J. Phys. Chem. B*, 2013, **117**, 1210–1218.
13 K. Kim, X. Xu, J. Guo and D. L. Fan, *Nat. Commun.*, 2014, 3632.
14 A. L. Balk, L. O. Mair, P. P. Mathai, P. N. Patrone, W. Wang, S. Ahmed, T. E. Mallouk, J. A. Liddle and S. M. Stavis, *ACS Nano*, 2014, **8**, 8300–8309.
15 A. Nourhani, P. E. Lammert, A. Borhan and V. H. Crespi, *Phys. Rev. E: Stat., Nonlinear, Soft Matter Phys.*, 2013, **87**, 050301.
16 S. van Teeffelen, U. Zimmermann and H. Löwen, *Soft Matter*, 2009, **5**, 4510–4519.
17 M. Mijalkov and G. Volpe, *Soft Matter*, 2013, **9**, 6376–6381.
18 S. J. Ebbens, G. A. Buxton, A. Alexeev, A. Sadeghi and J. R. Howse, *Soft Matter*, 2012, **8**, 3077–3082.
19 F. Kümmel, B. ten Hagen, R. Wittkowski, I. Buttinoni, R. Eichhorn, G. Volpe, H. Löwen and C. Bechinger, *Phys. Rev. Lett.*, 2013, **110**, 198302.
20 S. Fournier-Bidoz, A. C. Arsenault, I. Manners and G. A Ozin, *Chem. Commun.*, 2005, 441–443.
21 Y. Wang, S. T. Fei, Y. M. Byun, P. E. Lammert, V. H. Crespi, A. Sen and T. E. Mallouk, *J. Am. Chem. Soc.*, 2009, **131**, 9926–9927.

22 A. I. Campbell and S. J. Ebbens, *Langmuir*, 2013, **29**, 14066–14073.
23 S. Ebbens, D. A. Gregory, G. Dunderdale, J. R. Howse, Y. Ibrahim, T. B. Liverpool and R. Golestanian, *Europhys. Lett.*, 2014, **106**, 58003.
24 A. B. Pawar and I. Kretzschmar, *Langmuir*, 2008, **24**, 355–358.
25 S. Ebbens, R. A. L. Jones, A. J. Ryan, R. Golestanian and J. R. Howse, *Phys. Rev. E: Stat., Nonlinear, Soft Matter Phys.*, 2010, **82**, 015304.
26 S. M. Weekes, F. Y. Ogrin, W. A. Murray and P. S. Keatley, *Langmuir*, 2007, **23**, 1057–1060.
27 R. Golestanian, T. Liverpool and A. Ajdari, *Phys. Rev. Lett.*, 2005, **94**, 220801.
28 R. Golestanian, T. B. Liverpool and A. Ajdari, *New J. Phys.*, 2007, **9**, 126.
29 J. G. Gibbs and Y.-P. Zhao, *Appl. Phys. Lett.*, 2009, **94**, 163104.
30 N. H. Fletcher, *J. Chem. Phys.*, 1958, **29**, 572–576.